Electrochemistry Communications 74 (2017) 24–27

Contents lists available at ScienceDirect

Electrochemistry Communications

journal homepage: www.elsevier.com/locate/elecom

Nanosized palladium on holey graphene sheets incorporating P_xO_y for effective formic acid oxidation

Juan Wang [a,1], Detre Teschner [b], Xing Huang [b,*], Yuanying Yao [a,1], Marc Willinger [b], Lidong Shao [a,*], Robert Schlögl [b]

[a] Shanghai Key Laboratory of Materials Protection and Advanced Materials in Electric Power, Shanghai University of Electric Power, 2103 Pingliang Road, Shanghai 200090, China
[b] Department of Inorganic Chemistry, Fritz-Haber Institute of the Max Planck Society, Faradayweg 4-6, 14195 Berlin, Germany

ARTICLE INFO

Article history:
Received 20 October 2016
Received in revised form 22 November 2016
Accepted 22 November 2016
Available online 23 November 2016

Keywords:
Holey graphene
P_xO_y incorporation
Palladium nanoparticle
Metal–support interaction
HCOOH oxidation

ABSTRACT

A stack of basic structural carbon units incorporating phosphorus oxides (P_xO_y) at edges and internal defects is obtained and used as a support material for Pd nanoparticles, with the aim of creating an efficient electrocatalyst for HCOOH oxidation. In contrast to the lack of activity displayed by Pd supported on lyophilized and vacuum-annealed graphene oxides, Pd on holey graphene sheets incorporating P_xO_y (Pd/HGP_xO_y) shows efficient activity and stability in HCOOH oxidation. Surface analysis of fresh and reacted catalysts reveals that HCOOH oxidation is favored by Pd/HGP_xO_y due to the decreased Pd electron density caused by electron transfer from Pd to HGP_xO_y.

1. Introduction

Because the crossover flux through Nafion membranes of formic acid is lower than that of methanol, formic acid fuel cells offer exciting prospects for powering portable electronic devices [1]. Additionally, Pd anode catalysts show greater electrocatalytic activity for direct formic acid fuel cells with lower costs than Pt-based catalysts [2]. However, because of the ease of Pd oxidation, the electrocatalytic stability of Pd catalysts is not satisfactory. Secondary metals are commonly used to modify the electronic properties of Pd by forming alloys such as Pd—Co [3], Pd—Ni [4] and Pd—Au [5]. However, the erosion of binary-metal alloy catalysts in the acidic environment of fuel cells weakens the activity of these catalysts.

Recent works have reported that P doping can effectively improve the electrocatalytic activities of Pt and Pd catalysts. For example, C-supported Pt—Ru—P [6], Pt—Sn—P [7], Pt—P [8], Pd–PCNTs [9] and Pd—P [10] catalysts have been synthesized and used as anode or cathode electrocatalysts in fuel cells. Electrochemical measurements have shown that in the case of C-supported Pd—P catalysts [10], P doping can effectively promote formic acid electrooxidation through a direct pathway. However, modifying Pd with P on a C support for practical applications is challenging. Firstly, the mechanism by which the P or P_xO_y modifications affect HCOOH oxidation remains unclear. In the electrochemical field, the literature reports the existence of P as a simple substance and its interaction with C in forms of C—P bonds. Further interactions with supported metal particles take place as P–metal bonds. Such deductions are highly suspect in a great number of cases as we observed a high amount of P_xO_y in carbon networks even after high-temperature reduction treatment. Secondly, the utilization of C supports inevitably increases the thickness of the diffusion layer, thereby enhancing the mass-transfer resistance of the fuel molecules [11].

2. Experimental section

Pd/HGP_xO_y and Pd/HG were prepared as described below. Pd loading was carried out by the following route: palladium nitrate (ca. 40%Pd, Aldrich) was dissolved in ethanol and mixed with the supporting materials. Ultrasonication was carried out for 20 min and samples were dried by lyophilization. The samples were then collected and placed in a furnace for reduction treatment at 200 °C. X-ray diffraction (XRD) was performed using a Bruker D8 Advance XRD instrument with Cu-Kα radiation. An aberration-corrected JEOL JEM-ARM200CF transmission electron microscope was employed to investigate structural and chemical properties in STEM mode. X-ray photoelectron

* Corresponding authors.
E-mail addresses: xinghuang@fhi-berlin.mpg.de (X. Huang), lidong.shao@shiep.edu.cn (L. Shao).
[1] Juan Wang and Yuanying Yao contributed equally to this work.

http://dx.doi.org/10.1016/j.elecom.2016.11.012
1388-2481/

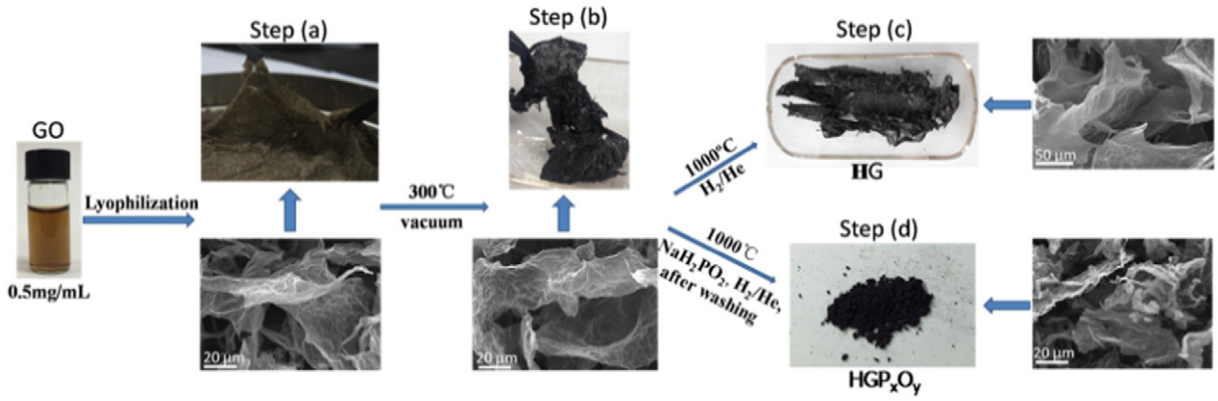

Fig. 1. Digital photos and SEM images of the obtained materials based on GO water solution.

spectroscopy (XPS) was conducted with a Thermo ESCALAB 250 XPS instrument using a monochromatic Al Kα source (1486.6 eV).

3. Results and discussion

In this work, graphite oxide was synthesized from purified natural graphite (SP-1, Bay Carbon) by the Hummers method [12]. Colloidal dispersion of graphene oxide (GO) sheets in water at a concentration of 0.5 g/L was achieved by 2 h of sonication. The digital photo of GO solution in Fig. 1 was taken after it had been kept stationary for one month. GO was extracted from the aqueous solution by lyophilization and the brown material obtained is shown together with its SEM characterization in Fig. 1(a). Subsequently, heat treatment was applied under vacuum at 300 °C; a digital photo of the resulting black material and its SEM image are shown in Fig. 1(b). Further heat treatment was conducted at 1000 °C under H_2/He atmosphere with and without sodium hypophosphite (NaH_2PO_2) to obtain graphene-based holey nanosheets incorporating P_xO_y and unmodified holey graphene nanosheets (HGP_xO_y and HG), respectively. After heat treatment in the presence of NaH_2PO_2, the material obtained was washed three times using distilled water and dried under vacuum at 60 °C. SEM images of the two heat-treated materials (HG and HG P_xO_y) are also shown in Fig. 1.

Fig. 2(a) shows the X-ray diffraction (XRD) patterns of the materials fabricated as described above. The peak at the lower $2\theta = 9.4°$ of lyophilized GO corresponds to an interlayer distance of 0.93 nm and results from the accommodation of various O-containing groups and water molecules during the graphite oxidation process [13,14]. After vacuum-annealing treatments, the absence of the 004 (21.6°), 100 (43.3°), and 101(44.5°) peaks shows that the materials are largely an X-ray amorphous, turbostratic mixture of basic structural units with many internal lattice defects. The absence of Pd peaks is due to the low loading of Pd dispersed in the nanoscale size range.

The structural evolution occurring during the lyophilization and heating processes is also reflected in the Raman spectra (Fig. 2b). After the 1000 °C annealing treatment, the ID/IG intensity ratio of HG and HGP_xO_y increased compared to that of the GO obtained in steps (a) and (b). This change suggests that holey structural units with increased internal lattice defects are generated upon reduction of the GO.

Pd with a large dispersion and narrow size distribution (3.3 ± 0.2 nm) was then deposited onto the HG and HGP_xO_y supports in low loadings (3 ± 0.2 wt%, measured by inductively coupled plasma (ICP)). To investigate the support effect, lyophilized GO (step a) and vacuum treated GO (step b) were used to support Pd. Fig. 2(c) displays a high-resolution transmission electron microscope (HRTEM) image of a metallic Pd particle with distinct edges on HGP_xO_y. The crystal planes and interplanar distances, as well as the acute angles, are labeled adjacent to the corresponding Pd particle. The insets show the fast Fourier transform of the local HRTEM image and the size distribution of the Pd particles.

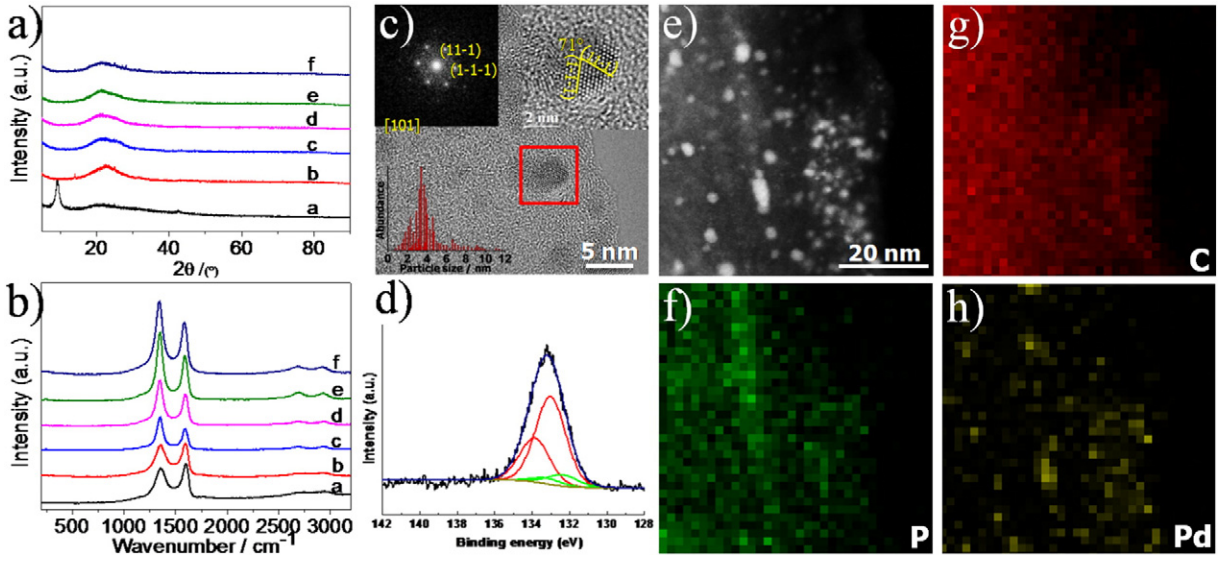

Fig. 2. (a) XRD and (b) Raman profiles with curves a, b, c, d corresponding to the materials obtained in step (a), step (b), step (c), and step (d) in Fig. 1. Curve e is Pd supported on HG, and f is Pd supported on HGP_xO_y. (c) HRTEM images of supported Pd particles. The insets show (top left) the fast Fourier transform of the local HRTEM image and (bottom) the Pd particle size distribution on HGP_xO_y. (d) XPS profile of P2p region of Pd/HGP_xO_y. (e), (f), (g), (h) STEM EDX mapping of Pd/HGP_xO_y.